A three-channel microfluidic device for generating static linear gradients and its application to the quantitative analysis of bacterial chemotaxis

Jinpian Diao,[a] Lincoln Young,[c] Sue Kim,[a] Elizabeth A. Fogarty,[a] Steven M. Heilman,[a] Peng Zhou,[c] Michael L. Shuler,[ad] Mingming Wu*[b] and Matthew P. DeLisa*[a]

Received 28th August 2005, Accepted 23rd November 2005
First published as an Advance Article on the web 13th December 2005
DOI: 10.1039/b511958h

We have developed a prototype three-channel microfluidic chip that is capable of generating a linear concentration gradient within a microfluidic channel and is useful in the study of bacterial chemotaxis. The linear chemical gradient is established by diffusing a chemical through a porous membrane located in the side wall of the channel and can be established without through-flow in the channel where cells reside. As a result, movement of the cells in the center channel is caused solely by the cells chemotactic response and not by variations in fluid flow. The advantages of this microfluidic chemical linear gradient generator are (i) its ability to produce a static chemical gradient, (ii) its rapid implementation, and (iii) its potential for highly parallel sample processing. Using this device, wildtype *Escherichia coli* strain RP437 was observed to move towards an attractant (*e.g.*, L-asparate) and away from a repellent (*e.g.*, glycerol) while derivatives of RP437 that were incapable of motility or chemotaxis showed no bias of the bacteria's distribution. Additionally, the degree of chemotaxis could be easily quantified using this assay in conjunction with fluorescence imaging techniques, allowing for estimation of the chemotactic partition coefficient (CPC) and the chemotactic migration coefficient (CMC). Finally, using this approach we demonstrate that *E. coli* deficient in autoinducer-2-mediated quorum sensing respond to the chemoattractant L-aspartate in a manner that is indistinguishable from wildtype cells suggesting that chemotaxis is insulated from this mode of cell–cell communication.

Introduction

Chemotaxis is the process by which cells move up or down a chemical gradient in response to an attractant or repellant and is a major factor in a bacterium's response to environmental changes.[1–3] In a uniform environment, bacteria swim by rotating their left-handed helical flagella bundle counter-clockwise using bidirectional, ion-driven rotary motors. When the flagellar motors switch to a clockwise rotation, the bundle is disrupted, and the bacterium undergoes a rapid change in swimming direction known as a tumble. Bacteria thus go through a 3D random walk composed of alternate runs and tumbles. When bacteria are challenged by concentration gradients of chemoeffectors, clockwise flagellar rotation and tumbling are suppressed. The random walk is therefore biased so that bacteria migrate up an attractant gradient or down a repellent gradient. Gradients are sensed as temporal changes in concentration by comparing the instantaneous concentration with the concentration the bacterium experienced a few seconds ago. Temporal comparisons involve an adaptation process in which ligand-occupied, membrane-spanning receptors are covalently methylated to reset their sensitivity and signaling capacity.[4,5]

There are at least six methods commonly used to study bacterial chemotaxis. The capillary assay, first created by Pfeffer[6] and later improved by Adler,[7] is the most commonly used especially for quantitative analysis.[8] The swarm plate is another commonly used assay introduced by Adler.[1] This technique allows isolation of non-motile or non-chemotactic mutants and allows relatively easy qualitative identification of chemoattractants. Temporal gradient assays are more quantitative in nature and are performed by imposing an abrupt step in concentration by simple addition or by more sophisticated means such as the temporal gradient apparatus[9] or the stopped-flow diffusion chamber.[10,11] Three-dimensional tracking is a single-cell assay whereby an automated microscope first developed by Berg and colleagues allows microscopic observation of the chemotactic behavior of a free-swimming cell.[12–16] Another microscopic technique involves the tethering of a cell to glass by a single flagellar filament enabling the real-time, continuous monitoring of the cell body's rotation and thus the operation of the corresponding flagellar motor.[17] More recently, microfluidic devices have been used to establish linear chemical gradients[18–20] and have been demonstrated for studying chemotaxis in both eukaryotes[21] and prokaryotes.[22] In these approaches, a stable gradient of chemoeffectors inside a microchannel was established *via* diffusion between parallel streams of liquid in laminar flow. The challenge in using such a "free diffusion" type channel is that it is impossible to separate

[a]*School of Chemical and Biomolecular Engineering, Cornell University, Ithaca, NY 14853, USA. E-mail: md255@cornell.edu; Fax: +1 (607) 255-9166; Tel: +1 (607) 254-8560*
[b]*Sibley School of Mechanical and Aerospace Engineering, Cornell University, Ithaca, NY 14853, USA. E-mail: mw272@cornell.edu*
[c]*Kionix, Inc. 36 Thornwood Drive, Ithaca, NY 14850, USA*
[d]*Department of Biomedical Engineering, Cornell University, Ithaca, NY 14853, USA*

Table 1 Bacterial strains and plasmids

Strains or plasmid	Genotype	Reference
RP437	Wildtype for motility and chemotaxis	23
U306	RP437 Δ*flhD*	28
U309	RP437 Δ*fliA*	28
RP2867	RP437 Δ*cheRB*	30
KX1485	RP437 *luxS*::Cm^r	35,43
MC1000	F- *araD139* Δ(*ara-leu*)*7697 galU galK* Δ*lacX74 rpsL thi*	44
VS184	MC1000 *qseC*::Tet^r	44
KX1486	RP437 *qseC*::Tet^r	This study
Plasmids		
pTrc99A	*trc* promoter, ColE1 ori, Amp^r	Amersham Pharmacia
pTrc-GFP	*gfpmut2* gene cloned in pTrc99A	This study

the effects of the fluid flow from those of the gradient when observing chemotaxis. As a result, it is difficult to know whether the movement of the cells in the channel is caused by variations in the fluid flow or by the cells chemotactic response. Additionally, the fluid flow limits the time the cells have to move (if it is a non-adherent cell) because the cell is flowing with the fluid and will exit the channel. Finally, since the flowing channel is not at steady state, the gradient profile is continuously changing throughout the length of the channel. This makes the gradient's profile and its effect on the chemotaxis of cells difficult to quantify.

In this study, we developed a microfluidic linear chemical gradient generator, and tested it in a study of bacterial chemotaxis. Our microfluidic assay is fundamentally different from those developed previously[18,19,22] in that we utilized a membrane-based three-channel configuration to generate the gradient. Fluid flow in one outer channel (source channel) has a constant chemical concentration, while the fluid flow in the other outer channel (sink channel) removes the chemicals in the system. Chemicals loaded into the source channel diffuse through the porous membrane and form a static linear gradient in the center channel. This configuration eliminates fluid flow from the center channel (where bacterial cells reside), which was unavoidable in previous microfluidic linear gradient generator studies.[18,19] Our configuration has obvious advantages for chemotaxis studies as it avoids possible hydrodynamic influences on the cells' chemotactic behavior. Another advantage of our three-channel configuration is that it eliminates the use of a syringe pump, which in turn (i) minimizes the complexities that are associated with low flow rate control and generation of delicate symmetric flow patterns; and (ii) reduces the cost of operation. The linear chemical gradient in the center channel is potentially able to persist infinitely provided that the flows in the side channels are maintained at a constant rate. Using this assay, we successfully monitored the random motility and chemotactic responses to L-aspartate (attractant) and glycerol (repellent) of wildtype *Escherichia coli* as well as mutants that were deficient in motility, chemotaxis and cell–cell communication.

Materials and methods

Strains and plasmids

All bacterial strains and plasmids used in this study are listed in Table 1.

Fabrication and assembly of devices

The schematic of the device is shown in Fig. 1. The core of the device is the three-channel network (Fig. 1A) which was fabricated from a piece of 16 μm × 20 μm size nitrocellulose membrane (BA85, 140 μm thickness, pore size 0.45 μm Schleicher & Schuell, Keene, NH). The three channels were cut out using a CO_2 laser (Model C10, Alase Technologies, Pepperell, MA) at 10% of maximum power and multiple passes. The sink and source channel widths are each 400 μm

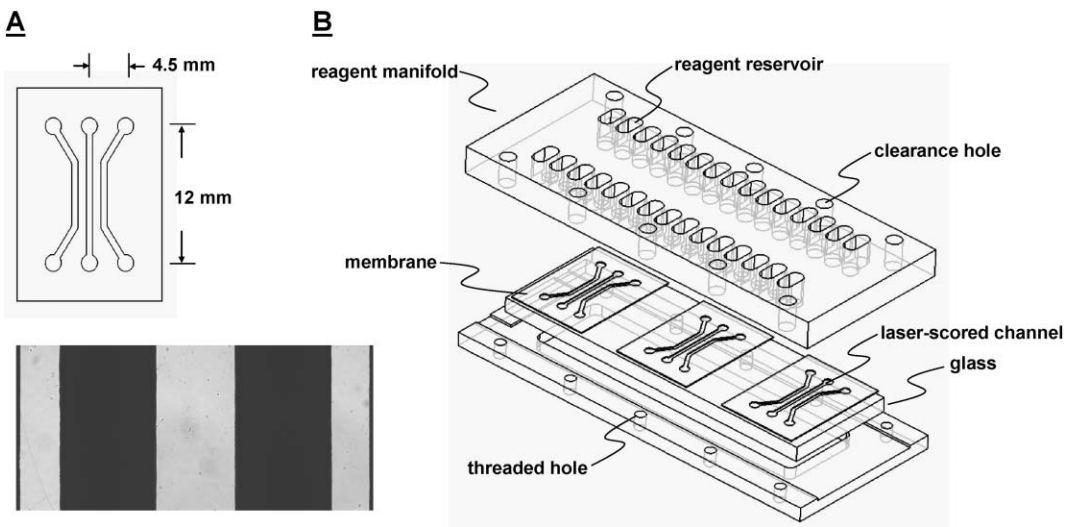

Fig. 1 Schematic diagram of the gradient generator device. (A) (top) Drawing of the 16 mm × 20 mm nitrocellulose membrane, in which three channels are cut out. The thickness of the membrane is ~140 μm; (bottom) micrograph of the three channels. The sink and source channels (or the two outer channels) have a width of 400 μm, and the center channel 800 μm. (B) An overview of the full device. The inlet or outlet (reservoir) of the channels is a 5 mm-deep well, having a width of 3 mm and a length of 7 mm.

and the center channel width is 800 μm. The depth of the channel varies between 135–155 μm depending on the way that the device is assembled. The top polycarbonate manifold was fabricated in-house using a vertical mill (Model 8020A, Sherline Products Inc., Vista, CA). A slide of Borofloat glass (McMaster-Carr, Cleveland, OH) was used underneath the nitrocellulose membrane. The stainless steel support was machined locally by Kionix, Inc. For a typical experiment, three pieces of membrane were sandwiched between the bottom glass and the top polycarbonate manifold (Fig. 1B) resulting in three functional chips. The sandwich was then secured to the stainless steel support with screws.

Gradient profile calibration

The gradient profile was probed using a 10^{-4} M fluorescein (Sigma, St. Louis, MO) solution. First, we monitored the light intensity emitted from the fluorescein solution enclosed in a 100 μm deep microfluidic channel and found that it was linear with the fluorescein concentration at concentrations $\leqslant 10^{-4}$ M. Then the device was calibrated as follows: 80 μl of 10^{-4} M fluorescein solution was loaded in the inlet of the source channel and 80 μl of deionized water was loaded into the inlet of the sink channel. Next, the fluorescence intensity of the sink, source and center channels was imaged every 5 min for ~1–2 h. All the components were soaked in deionized water for at least 30 min before the experiment. For flow rate measurements, we used 1 μm fluorescent beads (Duke Scientific), and measured the distance that each bead moved in two consecutive frames. For calibration, we used a CCD camera (Cascade 512B, 16bits, Photometric) in connection with an inverted fluorescence microscope (Olympus IX 51, 4X Olympus objective, NA = 0.1, FIFC filter cube).

Chemotaxis experiments

The *E. coli* strain RP437[23] and its derivatives were used for all chemotaxis experiments (see Table 1). All strains were transformed with plasmid pTrc-GFP, a pTrc99A-based expression vector (Amersham Pharmacia) containing the *gfpmut2* gene[24] downstream from the *trc* promoter. Plasmid-bearing cells were grown overnight in 10 ml Luria-Bertani (LB) medium supplemented with 100 μg ml^{-1} ampicillin (Sigma) at 30 °C in a 125 ml shake flask in an incubator shaker (G24 Environmental Incubator Shaker, New Brunswick Co., Edison, NJ). The overnight cultures were then used to inoculate fresh LB medium (10 ml) supplemented with 100 μg ml^{-1} ampicillin at a final OD_{600} of 0.05 followed by growth at 30 °C in a 125 ml shake flask in an incubator shaker. Once the OD_{600} reached 0.2, isopropyl thiogalactoside (IPTG, Sigma) was introduced into the culture at a final concentration of 1 mM to induce the *trc* promoter controlling the *gfpmut2* gene. Cells were harvested by centrifugation at 1500 × *g* at room temperature for two minutes once the OD_{600} reached 1.0. The cells were concentrated to an OD_{600} of 4.0 and resuspended in chemotaxis buffer by centrifugation at 1500 × *g* at room temperature twice for two minutes each time and kept at 30 °C until experiments were initiated. As a negative control, a proportion of live cells were suspended in chemotaxis buffer containing 0.5% sodium azide (Sigma).

Blank chemotaxis buffer and buffer containing a chemoeffector (80 μl) were loaded into the inlet reservoirs of the source channel and the sink channel, respectively. The concentrated bacteria solution was infused into the middle channel. The loaded devices were incubated in a closed humid chamber at 30 °C for 30 min. Following incubation, 100 time-lapsed images (200 ms exposure and 210 ms intervals between each picture) of the bacterial distribution in the middle channel were taken by using a 10× objective and a CCD camera (Model Retiga 1300, QImaging) mounted on the top of an up-right fluorescence microscope (Model BX51W1, Olympus America). Note that while an up-right microscope was used for these studies, the device could easily be imaged using an inverted camera if desired. The adsorption wavelength was set between 448 nm and 493 nm. The emission wavelength was set between 500 nm and 553 nm. ImageJ software was used to analyze the bacteria distribution across the middle channel.

Results and discussion

Calibration of the three-channel gradient generator

We first monitored the fluid flow driven by the hydrostatic force using 1 μm fluorescent beads. By tracking the bead velocity, we verified that there was no flow in the center channel (data not shown). A rough estimate of bead velocity gave us a flow rate of 10–25 μl h^{-1} in the sink and source channel when 80 μl of deionized water was added at the inlet. Using the vertical microtranslation stage, we also measured the channel height by focusing on the 1 μm beads that adhered to the upper and lower surfaces of the channel. The cell height varied slightly from run to run, ranging from 133–150 μm, and was dependent upon the clamping of the device during its assembly. We found that the linear concentration profile was established more robustly when the cell height was less than the membrane thickness, which was ~140 μm. Thus, for all the data shown below, the cell height was fixed to 133 μm. We define $t = 0$ as the time when 80 μl of fluorecein solution (10^{-4} M concentration) and 80 μl of deionized water were added to the inlet of sink and source channels respectively. We then monitored the fluorescence intensity in the sink, center and source channels at a 5 min time interval for ~1–2 h. A linear gradient of fluorecein dye was established in about 20 min (Fig. 2). This was consistent with the theoretical estimate of the time required for fluorescein dye to diffuse across a channel of 0.8 mm width, which was calculated as $(0.8\ cm)^2/D$, where $D = 10^{-6}\ cm^2\ s^{-1}$ for fluorecein dye.[25] To establish the concentration gradient, it was important that the membrane as well as the rest of the device were pre-wet. Since the membrane pore size is relatively large (0.45 μm), the hydrostatic pressure provided by the 80 μl at the inlet (~490 dyn cm^{-2}) was sufficient to drive the fluorescent solution through the membrane with no noticeable time delay. Notably, the time for the establishment of the linear profile was correlated to the cell height. For cell heights >140 μm, flows were observed between the glass/plastic and the membrane, and the establishment of the linear profile

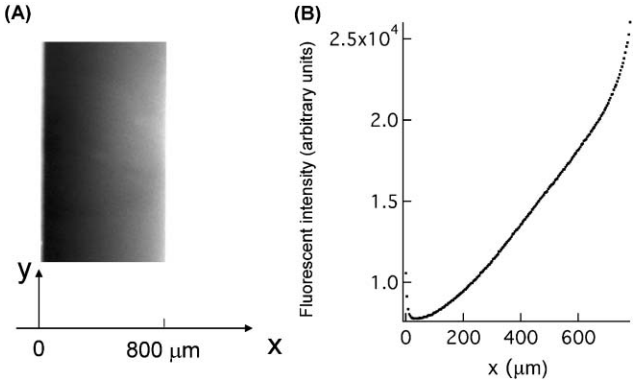

Fig. 2 (A) Image of the center channel at $t = 35$ min. The actual size of the image is 780 μm × 2048 μm. (B) The average fluorescence intensity at a fixed location along the x-direction.

decreased dramatically. In that situation, the linear profile was highly sensitive to the flow rate in the sink and source channel. This observation further justified our selection of 133 μm for the cell height for all experiments. Finally, as seen in Fig. 3, the fluorescence concentration difference across the center channel was between 1/10 − 1/6 (source concentration minus sink concentration) and repeated experiments confirmed that this was highly reproducible.

Response of *E. coli* to chemoattractants and chemorepellants

Wildtype *E. coli* strain RP437[23] and mutant strains derived from RP437 were loaded into the middle channel and challenged with a chemical gradient. The distribution profile of bacteria across the channel was determined by analyzing the fluorescence intensity profile of captured images based on the assumption that the signal intensity is proportional to the cell numbers. This information was then used to assess attractive *versus* repellent behavior of selected bacterial strains (see Figs. 4 and 5). Specifically, RP437 cells were observed to distribute symmetrically and broadly across the channel when

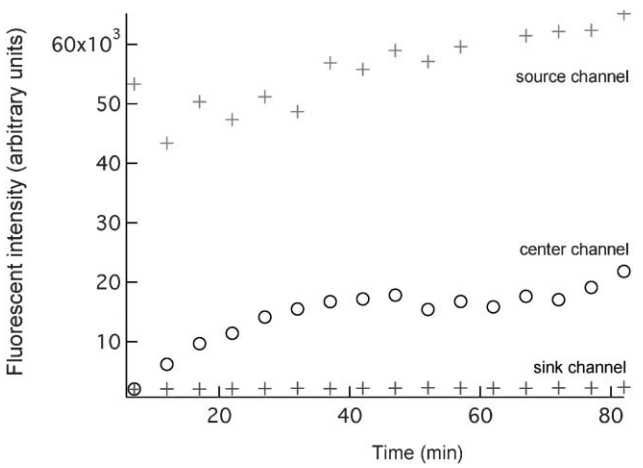

Fig. 3 Fluorescence intensity at a fixed y location for sink and source channels. For the center channel, fluorescence intensity is plotted as the difference across the channel. Here $t = 0$ is defined as the time when 80 μl of fluorescent solution and deionized water is added to the inlet of source and sink channel respectively.

the two outside channels were both filled with blank chemotaxis buffer (Fig. 4A). In contrast, RP437 migrated up known attractants such as L-aspartate gradients (10^{-4} M mm^{-1}, Fig. 4B) and α-methyl-DL-aspartate gradients (10^{-4} M mm^{-1}, Fig. 6A). When challenged with the same L-aspartate gradients, sodium azide-treated RP437 cells accumulated almost entirely in the middle of the channels (Fig. 4C) as sublethal concentrations of sodium azide are known to block motility *via* potent inhibition of bacterial respiratory chains.[26] Likewise, non-motile derivatives of RP437, namely U306 (RP437 Δ*flhD*) and U309 (RP437 Δ*fliA*) concentrated in the middle of the channels (Fig. 4D and E, respectively). These results are in agreement with our expectations as strains lacking *flhD* and *fliA*, both regulators of genes involved in flagellum formation, are known to be non-motile.[27–29] When the chemotactic mutant strain RP2867 (Δ*cheRB*) was challenged with an L-asparate gradient, cells diffused symmetrically and broadly across the middle channel (Fig. 4F) which was entirely consistent with previous reports that RP2867 cells run and tumble but are non-chemotactic.[30] To explore the effect of repellent, we challenged RP437 cells with a 10^{-4} M mm^{-1} concentration gradient of glycerol which is slightly below the reported threshold repellent concentration.[31] RP437 cells were observed to move down the gradient (Fig. 5A) whereas sodium-azide treated RP437 (data not shown), Δ*flhD* and Δ*fliA* (Fig. 5B and C, respectively) showed no glycerol-induced bias as evidenced by their positioning in the middle of the channels. Finally, RP2867 cells exposed to 10^{-4} M mm^{-1} glycerol were distributed broadly across the middle channel indicating no glycerol-induced bias (Fig. 4D). For these experiments, the reported gradients reflect the chemoeffector concentration difference between the source channel and sink channel. It should be noted, however, that the boundary value of the concentration gradient in the center channel is expected to be on the order of 1/6 the source concentration based on measurements for fluorescein above.

Interestingly, we consistently observed that the cell distribution across the center channel always peaked at the channel center when the cells were non-chemotactic, instead of a uniform spatial distribution (*e.g.*, Fig. 4D, E and F). This effect is likely caused by the fact that the cells are introduced to the channel by hydrodynamic flow. This non-uniformity of the cell distribution is known as Taylor-dispersion. It is caused by the fact that fluid flow moves slower close to the channel wall than in the center. Details of the underlying mechanism can be found in a paper by Taylor.[32]

Quantifying the chemotactic behavior

Two chemotaxis coefficients, the chemotaxis partition coefficient (CPC) and chemotaxis migration coefficient (CMC), were previously defined by Mao *et al.*[22] to indicate the direction and degree of migration of bacteria in a geometrical configuration that was similar to the one used in our study. To calculate CPC and CMC, the channel was divided in half with intensity values obtained for the half-channel nearest to the channel filled with chemoeffectors assigned as positive and values obtained for the opposite half-channel assigned as negative. CPC is defined as the net value obtained by

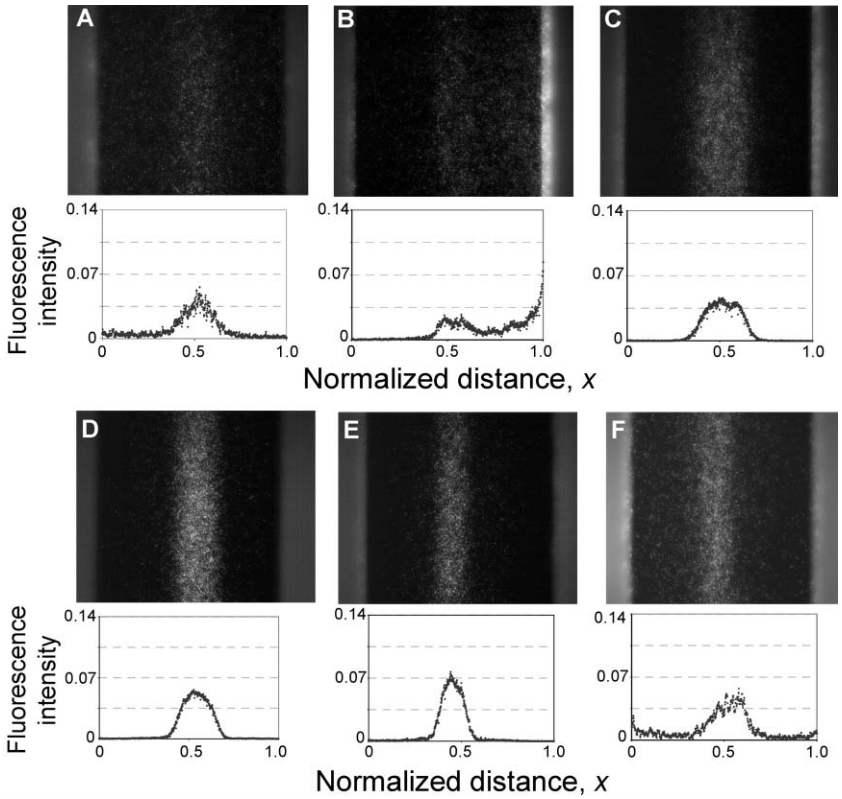

Fig. 4 Bacterial response to chemoattractant challenge. The left channel of the device was always filled with blank chemotaxis buffer. The right channel was filled with chemotaxis buffer containing 10^{-4} M L-aspartate. The center channel was infiltrated with bacteria. The following was added to the right and center channel respectively: (A) blank buffer and RP437; (B) 1×10^{-4} M L-aspartate and RP437; (C) 1×10^{-4} M L-aspartate and sodium azide-treated RP437; (D) 1×10^{-4} M L-aspartate and RP437 Δ*flhD*; (E) 1×10^{-4} M L-aspartate and RP437 Δ*fliA*; (F) 1×10^{-4} M L-aspartate and RP437 Δ*cheRB*. Histograms represent normalized fluorescence intensity across the channel plotted *versus* normalized position in the channel. Fluorescence values obtained at each position x across the channel were normalized to the total fluorescence in the channel.

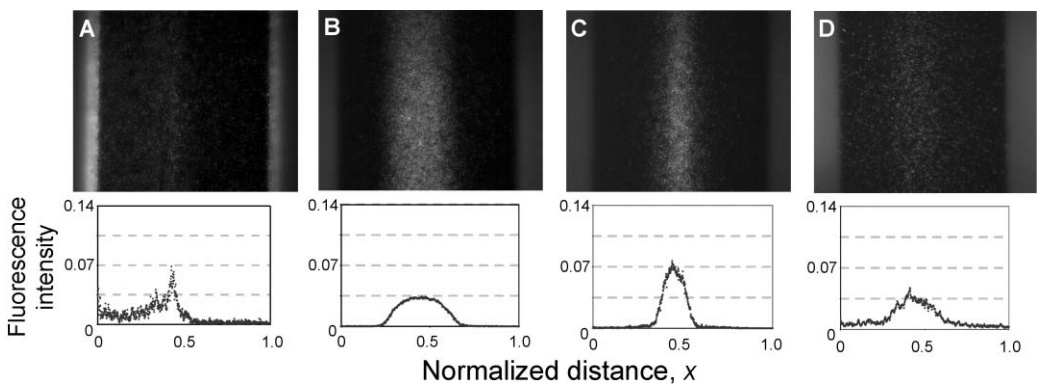

Fig. 5 Bacterial response to chemorepellent challenge. The left channel of the device was always filled with blank chemotaxis buffer. The right channel was filled with chemotaxis buffer containing 10^{-4} M glycerol. The center channel was infiltrated with bacteria. The following was added to the right and center channel respectively: (A) 1×10^{-4} M glycerol and RP437; (B) 1×10^{-4} M glycerol and RP437 Δ*flhD*; (C) 1×10^{-4} M glycerol and RP437 Δ*fliA*; (D) 1×10^{-4} M glycerol and RP437 Δ*cheRB*. Histograms represent normalized fluorescence intensity across the channel plotted *versus* normalized position in the channel. Fluorescence values obtained at each position x across the channel were normalized to the total fluorescence in the channel.

integrating all polarized cell numbers across the channel, normalized by the total cell number in the channel. CMC integrates the migration distance information. Specifically, CMC was defined as follows:

$$\mathrm{CMC} = \mathrm{sum}(I \times (x - w/2))/\mathrm{sum}(I)/(w/2),$$

where I is the light intensity, w is channel width and x is the polarized cell number at a position in the channel weighted by its distance as a fraction of the half-channel width (see Fig. 2). Fig. 6A shows the distribution of RP437 cells responding to 10^{-4} M mm^{-1} α-methyl-DL-aspartate. As was seen above for L-aspartate challenge, the bacteria biased their swimming towards

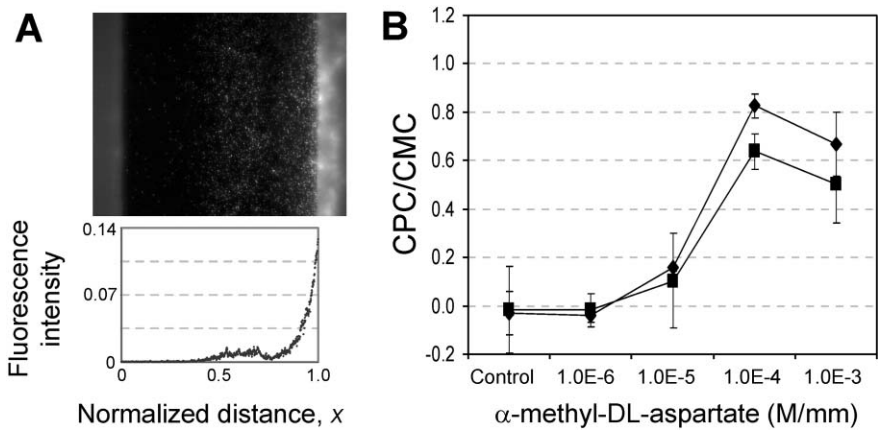

Fig. 6 (A) Response of RP437 to 10^{-4} M mm^{-1} α-methyl-DL-aspartate. Histogram represents normalized fluorescence intensity across the channel plotted *versus* normalized position in the channel. Fluorescence values obtained at each position x across the channel were normalized to the total fluorescence in the channel. (B) The chemotaxis partition coefficient (CPC, ◆) and chemotaxis migration coefficient (CMC, ■) for RP437 cells responding to varying concentrations of α-methyl-DL-aspartate. Control experiments were performed using blank chemotaxis buffer. Experimental data is reported as the average of three replicate chemotaxis experiments.

α-methyl-DL-aspartate. Fig. 6B depicts the CPC and CMC of RP437 cells responding to a range of different α-methyl-DL-aspartate concentration gradients. At high concentration gradients of α-methyl-DL-aspartate (10^{-5} M mm^{-1}–10^{-3} M mm^{-1}), CPCs and CMCs are positive. These values are consistent with the notion that Tar receptors (taxis toward aspartate and its analogs) located in the membranes of RP437 cells[33] enable cells to sense and migrate up the α-methyl-DL-aspartate concentration gradients. At low concentration gradients (10^{-6} M mm^{-1}), the absolute value of CPC and CMC are negative, but comparable with the CPC and CMC of blank buffer, indicating that this low concentration may be at the detection threshold of the assay. CPC and CMC increase as the concentration gradients become steeper (from 10^{-5} M mm^{-1} to 10^{-4} M mm^{-1}) but then decrease at the steepest gradients (from 10^{-4} M mm^{-1} to 10^{-3} M mm^{-1}). This is consistent with the finite number of receptors on a cell's membrane, which are saturated when cells are in a highly concentrated solution containing chemoeffectors.[33] At saturating concentrations of chemoeffector, cells no longer sense ever-increasing concentrations of the attractant and, as a result, do not move up the concentration gradient.

Effect of quorum signal autoinducer-2 on chemotaxis in *E. coli*

It has previously been hypothesized that cell–cell communication (aka quorum sensing) might play an important role in bacterial chemotaxis.[34,35] In *E. coli*, cell–cell communication is thought to be mediated in part by the autoinducer-2 (AI-2) signaling molecule,[36,37] which was recently shown to be a furanosyl borate diester.[38] Genome-wide transcriptional profiling indicates that a number of genes respond to the AI-2 signal,[39–41] many of which are connected to chemotaxis, flagellar synthesis and motility. Indeed, deletion of the AI-2 synthase gene, *luxS*, has been observed to decrease the motility of enterohemorrhagic *E. coli* (EHEC) O157:H7 using a semi-solid plate motility assay.[41] Along similar lines, EHEC and K-12 *E. coli* carrying insertions in *qseC*, a gene encoding an AI-2-responsive sensor kinase, were significantly reduced in motility relative to wildtype *E. coli*. These data suggest that a connection exists between quorum sensing and motility however the extent to which quorum sensing and chemotaxis are linked has not been tested. Therefore, we explored the use of our three-channel gradient generator to determine whether bacterial cell–cell communication affects motility and/or chemotaxis in *E. coli*.

For these studies, RP437 cells and mutants derived from RP437 that contained insertions in either *luxS* or *qseC* (strains KX1485 and KX1486, respectively) were infused into the microfluidic device and challenged with L-aspartate. Both mutant strains were highly motile (data not shown) and exhibited chemotactic behavior in response to 10^{-4} M mm^{-1} L-aspartate that was virtually indistinguishable from wildtype RP437 cells exposed to the same L-aspartate gradient (shown for RP437 *versus* KX1485, compare insets in Fig. 7A and B). Moreover, when quorum sensing mutants were challenged with a range of L-aspartate concentration gradients, we observed nearly identical profiles for the chemotactic response as quantified by CPC/CMC analysis of image data taken from gradient generator experiments. Specifically, both RP437 and KX1485 moved towards L-aspartate as indicated by the positive CPC and CMC profiles for L-aspartate concentrations between 10^{-5} M mm^{-1}–10^{-3} M mm^{-1} (Fig. 7A and B). Thus, there appears to be no measurable difference in the chemotactic behavior of wildtype and *luxS*-deficient *E. coli* mutants as determined by our microfluidic gradient generator and CPC/CMC analysis.

Conclusions

In the present study, we developed a plastic-membrane-glass sandwiched three-channel microfluidic chip that was demonstrated to be useful for bacterial chemotaxis studies. The most noteworthy aspect of our device is its ability to generate a static, linear chemical gradient in the center channel. As a result, cell movement in the center channel is caused solely by cellular motility and/or chemotaxis and not by variations in the fluid flow. Flow-based and migratory effects can in fact be

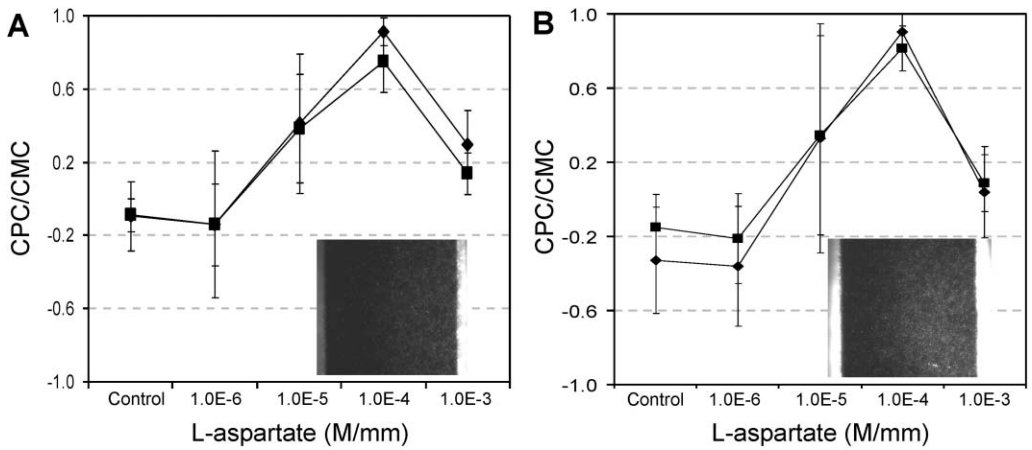

Fig. 7 The experimental CPC (◆) and CMC (■) of RP437 and KX1485 (RP437 Δ*luxS*) responding to varying concentration gradients of L-aspartate. Control experiments were performed using blank chemotaxis buffer. Experimental data is reported as the average of three replicate chemotaxis experiments. Figure insets depict representative images of RP437 and KX1485 in response to L-aspartate.

differentiated for adherent cells,[42] but can confound chemotactic analysis of non-adherent cells. Accordingly, the static nature of our gradient was found to be particularly useful when monitoring chemotaxis of non-adherent cells such as the gram-negative bacterium *E. coli*. Another important feature of the device is that it utilizes hydrostatic force for fluid delivery to constantly refresh the chemoeffector source and sink in the outer channels and molecular diffusion for spatial gradient generation. The advantage of hydrostatic fluid delivery and molecular diffusion is that our device is: (i) extremely easy to implement as it does not require low flow control or delicate symmetric flow patterns which can introduce additional experimental complexities; and (ii) inexpensive. One limitation of our prototype device is that run-to-run variations arise owing to the screwing procedure used to assemble the bottom glass and the top polycarbonate manifold. This was largely resolved by measuring the cell height prior to each run and ensuring a height of $\sim$140 μm, however a cell height control (*e.g.*, addition of a spacer) will be employed in the future. Further reduction of variability can be achieved by introduction of a flow controller that maintains a constant height differential between the inlet and outlet reservoirs.

Due to the characteristics outlined above, we have found that this device is extremely well-suited to the study of bacterial chemotaxis. Specifically, we observed wildtype RP437 to move towards an attractant (10^{-4} M mm^{-1} L-asparate) and away from a repellent (10^{-4} M mm^{-1} glycerol) while derivatives of RP437 that were incapable of motility (RP437 Δ*flhD* and RP437 Δ*fliA*) or chemotaxis (RP437 Δ*cheRB*) showed no measurable bias of the bacteria's distribution. Overall, the strength of this device is its rapid and facile implementation, its ability to generate a static linear chemical gradient and its future potential for highly parallel sample processing. Furthermore, even though only bacterial chemotaxis assays were demonstrated in this study, the three-channel gradient generator should easily be extended to the study of mammalian cell chemotaxis, especially since there was no flow in the middle channel where the gradient was established.

Interestingly, derivatives of RP437 that could not produce the diffusible quorum signal molecule AI-2 (strain KX1485) or that could not respond to the AI-2 signal due to loss of the QseC sensor kinase (strain KX1486) exhibited chemotactic behavior that was indistinguishable from wildtype cells. Collectively, our data demonstrate that the use of the gradient generator in conjunction with CPC/CMC analysis can be used to quantify chemotaxis in a manner that is less straightforward using traditional chemotaxis assays. It is also noteworthy that, because the detection method (*e.g.* image acquisition and analysis) for our novel chemotactic assay is entirely non-invasive, the distribution of cells across the generated gradient can be monitored continuously to provide dynamic information of bacterial chemotactic behavior.

Acknowledgements

This work was supported by funds from the New York State Office of Science, Technology and Academic Research (NYSTAR) to M.L.S, M.W. and to M.P.D. (in the form of a James D. Watson Investigator Award). The authors would like to thank Dr John Parkinson, Dr Uri Alon and Dr Peter Wolanin for kindly providing RP437 and several of its derivatives and Dr Vanessa Sperandio for providing strain VS184. We thank the NSF-funded Cornell Nanobiotechnology Center for providing access to laboratory space for the microscopy experiments. We would also like to thank Kionix, Inc. for partial support of J. Diao and the Cornell Learning Initiatives for Future Engineers (LIFE) Program for providing a stipend to S. Kim.

References

1 J. Adler, *Science*, 1966, **153**, 708–716.
2 M. Eisenbach, *Chemotaxis*, Imperial College Press, London, 2004.
3 R. M. Macnab, in *Escherichia coli and Salmonella: Cellular and Molecular Biology*, ed. F. C. Neidhardt, J. L. Ingraham, E. C. C. Lin, K. B. Low, B. Magasanik, W. S. Reznikoff, M. Riley , M. Schaechter and H. E. Umbarger, American Society of Microbiology, Washington, DC, 1996, pp. 732–759.
4 R. M. Weis, S. Chasalow and D. E. Koshland, Jr., *J. Biol. Chem.*, 1990, **265**, 6817–6826.

5 D. E. Koshland, Jr., D. A. Sanders and R. M. Weis, *Cold Spring Harbor Symp. Quant. Biol.*, 1988, **53**, 1, 11–17.
6 W. Pfeffer, *Unters. Botan. Inst. Tubingen*, 1888, **2**, 582–661.
7 J. Adler, *J. Gen. Microbiol.*, 1973, **74**, 77–91.
8 P. Lewus and R. M. Ford, *Biotechnol. Bioeng.*, 2001, **75**, 292–304.
9 R. M. Macnab and D. E. Koshland, Jr., *Proc. Natl. Acad. Sci. U.S.A.*, 1972, **69**, 2509–2512.
10 R. M. Ford and D. A. Lauffenburger, *Biotechnol. Bioeng.*, 1991, **37**, 661–672.
11 R. M. Ford, B. R. Phillips, J. A. Quinn and D. A. Lauffenburger, *Biotechnol. Bioeng.*, 1991, **37**, 647–660.
12 H. C. Berg, *Rev. Sci. Instrum.*, 1971, **42**, 868–871.
13 H. C. Berg, *Adv. Opt. Electron Microsc.*, 1978, **7**, 1–15.
14 H. C. Berg, *E. coli in motion*, Springer-Verlag, 2004.
15 H. C. Berg and D. A. Brown, *Nature*, 1972, **239**, 500–504.
16 H. C. Berg and D. A. Brown, *Antibiotics Chemother.*, 1974, **19**, 55–78.
17 M. Silverman and M. Simon, *Nature*, 1974, **249**, 73–74.
18 S. K. Dertinger, D. T. Chiu, N. Li Jeon and G. M. Whitesides, *Anal. Chem.*, 2001, **73**, 1240–1246.
19 N. Li Jeon, S. K. Dertinger, D. T. Chiu, I. S. Choi, A. D. Stroock and G. M. Whitesides, *Langmuir*, 2000, **16**, 8311–8316.
20 F. Lin, W. Saadi, S. W. Rhee, S.-J. Wang, S. Mittal and N. L. Jeon, *Lab Chip*, 2004, **4**, 164–167.
21 N. Li Jeon, H. Baskaran, S. K. Dertinger, G. M. Whitesides, L. Van der Water and M. Toner, *Nat. Biotechnol.*, 2002, **20**, 826–830.
22 H. Mao, P. S. Cremer and M. D. Manson, *Proc. Natl. Acad. Sci. U.S.A.*, 2003, **100**, 5449–5454.
23 J. S. Parkinson, *J. Bacteriol.*, 1978, **135**, 45–53.
24 B. P. Cormack, R. H. Valdivia and S. Falkow, *Gene*, 1996, **173**, 33–38.
25 A. W. Moore, Jr. and J. W. Jorgenson, *Anal. Chem.*, 1993, **65**, 3550–3560.
26 H. Lunsdorf and H. U. Schairer, *Microbiology*, 2001, **147**, 939–947.
27 S. Kalir, J. McClure, K. Pabbaraju, C. Southward, M. Ronen, S. Liebler, M. G. Sureth and U. Alon, *Science*, 2001, **292**, 2080–2083.
28 S. Kalir and U. Alon, *Cell*, 2004, **117**, 713–720.
29 P. Aldridge and K. T. Hughes, *Curr. Opin. Microbiol.*, 2002, **5**, 160–165.
30 J. S. Parkinson and S. E. Houts, *J. Bacteriol.*, 1982, **151**, 106–113.
31 M. Eisenbach, C. Constantinou, H. Aloni and M. Shinitzky, *J. Bacteriol.*, 1990, **172**, 5218–5224.
32 G. I. Taylor, *Proc. R. Soc. London, Ser. A*, 1953, **219**, 186–203.
33 M. S. Springer, M. F. Goy and J. Adler, *Proc. Natl. Acad. Sci. U.S.A.*, 1977, **74**, 3312–3316.
34 E. Ben Jacob, I. Becker, Y. Shapira and H. Levine, *Trends Microbiol.*, 2004, **12**, 366–372.
35 S. Park, P. M. Wolanin, E. A. Yuzbashyan, P. Silberzan, J. B. Stock and R. H. Austin, *Science*, 2003, **301**, 188.
36 B. L. Bassler, *Cell*, 2002, **109**, 421–424.
37 K. B. Xavier and B. L. Bassler, *Curr. Opin. Microbiol.*, 2003, **6**, 191–197.
38 X. Chen, S. Shauder, N. Potier, A. Van Dorsselaer, I. Pelczer, B. L. Bassler and F. M. Hughson, *Nature*, 2002, **415**, 545–549.
39 M. P. DeLisa, C. F. Wu, L. Wang, J. J. Valdes and W. E. Bentley, *J. Bacteriol.*, 2001, **183**, 5239–5247.
40 D. Ren, L. A. Bedzyk, R. W. Ye, S. M. Thomas and T. K. Wood, *Biotechnol. Bioeng.*, 2004, **88**, 630–642.
41 V. Sperandio, A. G. Torres, J. A. Giron and J. B. Kaper, *J. Bacteriol.*, 2001, **183**, 5187–5197.
42 G. M. Walker, J. Sai, A. Richmond, M. Stremler, C. Y. Chung and J. P. Wikswo, *Lab Chip*, 2005, **5**, 611–618.
43 S. Park, P. M. Wolanin, E. A. Yuzbashyan, H. Lin, N. C. Darnton, J. B. Stock, P. Silberzan and R. H. Austin, *Proc. Natl. Acad. Sci. U.S.A.*, 2003, **100**, 13910–13915.
44 V. Sperandio, A. G. Torres and J. B. Kaper, *Mol. Microbiol.*, 2002, **43**, 809–821.

